Optik - International Journal for Light and Electron Optics 208 (2020) 164061

Contents lists available at ScienceDirect

Optik

journal homepage: www.elsevier.com/locate/ijleo

Original research article

Comparison of efficiency analysis of perovskite solar cell by altering electron and hole transporting layers

Syeda Ammara Shabbir*, Zuha Azher, Hamid Latif

Forman Christian College (A Chartered University), Lahore 54600, Pakistan

ARTICLE INFO

Keywords:
Perovskite solar cell
Photovoltaic technology
Hole transport material free
Mesoporous titanium dioxide

ABSTRACT

The methylamine lead halide perovskites as the light harvesting material in solar devices are emerging and promising due to their easy manufacturing process and large photovoltaic efficiency. Generally perovskite solar cells consist of a structure in which the perovskite light absorbing layer is sandwiched between electron and hole transporting layers (ETLs and HTLs). Herein we report four types of perovskite ($CH_3NH_3PbBr_3$) solar cells which were fabricated in the absence and presence of electron transporting layer (Titanium dioxide (TiO_2)) and hole transporting layer (2,2′,7,7′-Tetrakis[*N,N*-di(4-methoxyphenyl)amino]-9,9′-pirobifluorene (Spiro-OMeTAD)). Efficiency comparison analysis of fabricated solar cells was performed in the absence and presence of electron and hole transporting layers. All layers were deposited by spin-coating method. Different analysis using XRD, SEM, UV and IV measurements were carried out for all samples. Maximum power conversion efficiency of 13.8 % was obtained.

1. Introduction

In recent years methylammonium lead halides with general formula ABX_3, where A is organic, B is inorganic and X_3 is trihallide, have gained much attention in photovoltaic applications because of high power conversion efficiency (PCE) of over 28 %. The major benefits of these semiconducting perovskite materials include low cost, easy fabrication, high diffusion length, high charge carrier mobility, comparatively low band gap, ambipolar transport behavior and favorable light harvesting properties [1,2].

In a general perovskite solar cell, when incident light gets absorbed by perovskite layer, electron and holes are generated and injected into n-type and p-type semiconducting materials respectively. This charge carriers transportation through different pathways play key role in attaining high PCE [3]. Consequently the selection of materials and their surface structure significantly affects the PCE. Currently a lot of research work has been reported for hole transport material (HTM) free perovskite solar cells. In HTM free solar cell, lead halide perovskites can transport holes in addition to its light harvesting functionality. Elimination of HTM layer in Perovskite solar cell (PSCs) has several advantages such as cost reduction, simple fabrication without oxidation and providing higher stability. However exclusion of such an important HTM layer in solar cell structure leads to reduced photovoltaic efficiency [4]. However, recent HTM free perovskite solar cells have achieved 17.89 % PCE [5]. To further simplify the device structure and to get rid of complex electron transporting layer (ETL), such as compact TiO_2, mesoporous TiO_2, SnO_2 and ZnO etc, a relatively new ETL free device structure is recently introduced [1,6]. Therefore, several efforts have investigated the major challenges of PSCs, such as device reproducibility and improving operational stability [5–7] All the contact layers are critical, Their elimination might be limiting the device performance of state-of-the-art devices however increasing reproducibility and stability. In this contribution we

* Corresponding author.
E-mail address: ammaraanwar@fccollege.edu.pk (S.A. Shabbir).

https://doi.org/10.1016/j.ijleo.2019.164061
Received 9 November 2019; Accepted 11 December 2019

have focused on the role of the electron and hole transport layers regarding electronics and optics.

In this project efficiency comparison of four perovskite solar cells is performed, which are fabricated in the absence and presence of ETL and HTM layers. Titanium dioxide (TiO_2) worked as ETL, methyl ammonium lead bromide ($CH_3NH_3PbBr_3$) as perovskite and 2, 20,7,70tetrakis(*N,N*-di-p-ethoxyphenylamino)-9,90-spirobifluorene (Spiro-OMeTAD) as HTM. A compact layer of TiO_2 is deposited between FTO and ETL. The purpose of compact TiO_2 layer is to prevent charge recombination between FTO and perovskite layer. Compact TiO_2 also known as blocking layer plays a crucial part in the PSC because it prevents carriers from directly contacting the conducting substrate (FTO) and thereby shunting the device [7]. Prevention of such recombination is essential as it leads to lower charge collection efficiency, which in turn lowers short circuit current (Jsc) and fill factor (FF) in the current voltage measurements of PSC. Mesoporous TiO_2 as ETL plays an efficient role in efficiency enhancement. This is due to increased surface area of mesoporous structures so that the complete structure can interact with atoms, ions and molecules [8].

2. Experimental

2.1. Chemicals and apparatus

Acetone, ethanol, isopropanol, distilled water, titanium isopropoxide, TiO_2 paste (Dyesol 18 NR-T), methyl amine, hydrobromic acid, lead bromide, dimethyl formamide, 2,20,7,70-tetrakis(*N,N*-di-p-ethoxyphenylamino)-9,90-spirobifluorene (spiro-OMeTAD) and silver paste were used. X-ray diffraction (XRD), scanning electron microscope (SEM) were used for surface structure characterization. UV–vis spectroscopy was utilized for optical properties and bandgap measurements and solar simulator for current voltage measurements.

2.2. Fabrication of photovoltaic devices

Flourine doped tin oxide (FTO) glasses were used as substrate in all four perovskite solar cells. All the substrates were sequentially washed in ultrasonic bath with ethanol, isopropanol and distilled water for 10 min each. After bathing, the substrates were allowed to dry at room temperature. For deposition of compact TiO_2 layer, precursor solution was prepared by stirring 0.15 M of titanium isopropoxide in ethanol for 1 h. This precursor solution was spin coated at 3000 rpm (30 s). The deposited film was thermally annealed at 450 °C for 2 h [9]. In the next step, mesoporous TiO_2 as ETL was deposited. Precursor solution was prepared by diluting TiO_2 paste (Dyesol 18 NR-T) in ethanol at 1:35 by weight. The solution was spin coated at 2000 rpm (50 s) and heated at 500 °C for 30 min [10]. The deposition of perovskite, methylammonium lead bromide ($CH_3NH_3PbBr_3$), was performed in two steps. At first methyl ammonium bromide (CH_3NH_3Br) was prepared by mixing methyl amine (40 % in methanol) with hydrobromic acid (48 % in water) in 1:1 M ratio in 100 ml beaker under continuous stirring for 2 h. The solution was heated in vacuum oven for 24 h at 60 °C. White colored powder was obtained after heating. A 40 % weight solution of $CH_3NH_3PbBr_3$ was prepared by mixing lead bromide $PbBr_2$ and methyl ammonium bromide CH_3NH_3Br in equimolar ratio in dimethylformamide (DMF). The solution was stirred for 1 h and then deposited by spin coating at 500 rpm (5 s) at first and then at 3000 rpm (30 s). The substrate was heated at hot plate for 15 min at 500 °C [11,12]. For deposition of HTM layer, spiro-OMeTAD was diluted in dimethyl formamide (DMF) (120 mg/ml). Solution was spin coated at 1000 rpm (9 s) at first and then at 4000 rpm (30 s). Substrate was heated at hot plate for 15 min at 120 °C [13]. The top most electrode was prepared by depositing silver paste using doctor blade method. Schematic diagrams of all four devices are shown in Fig. 1.

2.3. Results and discussions

X-ray diffraction (XRD) patterns of compact TiO_2, mesoporous TiO_2 and $CH_3NH_3PbBr_3$ are shown in Fig. 2(a)–(c) respectively. All XRD patterns shows the corresponding crystal structures with required peaks at specific angles. XRD pattern of $CH_3NH_3PbBr_3$ reveals the cubic crystalline structure of perovskite [14]. Phase purity of the cubic $CH_3NH_3PbBr_3$ structure is clear from sharpness of XRD peaks. For compact and mesoporous TiO_2, peak positions and their corresponding intensities of diffraction lines matches with the standard diffraction pattern of anatase and rutile phase TiO_2. XRD pattern of compact TiO_2 shows peaks at 2Θ values of 27, 34, 52 and 62, corresponding to (110), (101), (211), (220) and (002) planes respectively, indicating the rutile phase. Similarly peaks at 2Θ values of 25, 38, 48, 54, 55 and 63, corresponding to (101), (004), (200), (105), (211) and (204) planes indicates anatase phase of mesoporous TiO_2 [15,16]. Average grain size is calculated from peaks of XRD data using Debye Scherrer formula given below:

$$D = \frac{K\lambda}{\beta cos\theta}$$

Where D is grain size, K is constant (0.89), λ is wavelength of X-ray (0.154 nm), β is intensity at full width half maximum (FWHM) and Θ is Bragg's angle of diffraction. Average grain size calculated for compact TiO_2, mesoporous TiO_2 and $CH_3NH_3PbBr_3$ was 16 nm, 12 nm and 20 nm respectively.

The surface morphologies of the fabricated layers were analyzed by scanning electron microscope (SEM). SEM image in Fig. 3a shows the sphere shaped compact TiO_2 nanoparticles which are densely stacked together. Dense stacking fulfills the purpose of compact layer to prevent hole recombination. If the layer is not compact, then small dark holes are seen on the image. Presence of holes can lead to hole recombination which reduces the device efficiency. The absence of holes in the SEM images of compact titanium dioxide TiO_2 layer demonstrates the synthesis of efficient layer which is sufficiently compact. Average particle size of

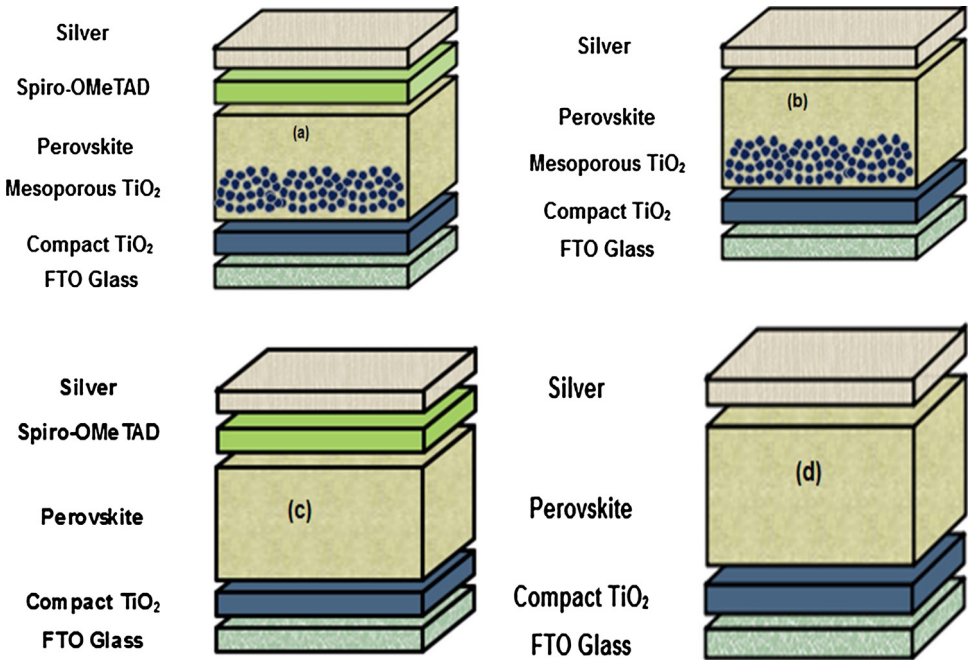

Fig. 1. Schematic illustration of fabricated solar devices : (a) device 1. (b) Device 2. (c) Device 3. (d) Device 4.

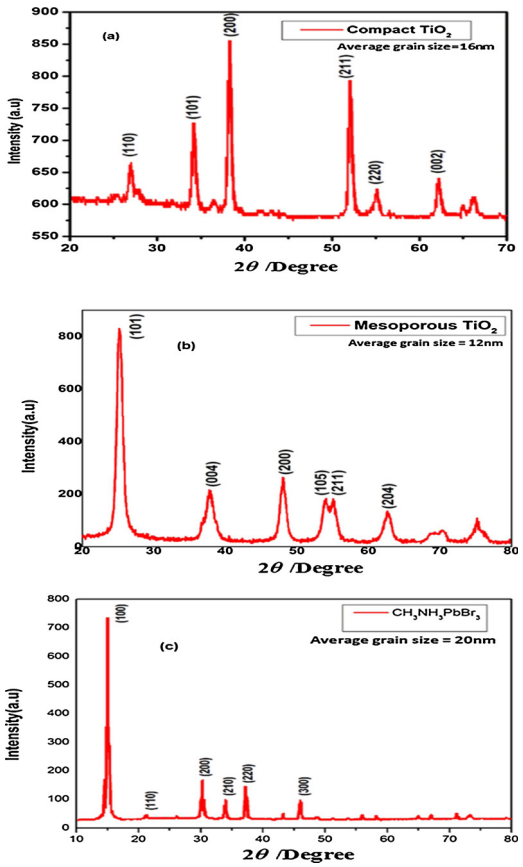

Fig. 2. XRD diffraction pattern. (a) compact TiO_2. (b) Mesoporous TiO_2. (c) $CH_3NH_3PbBr_3$.

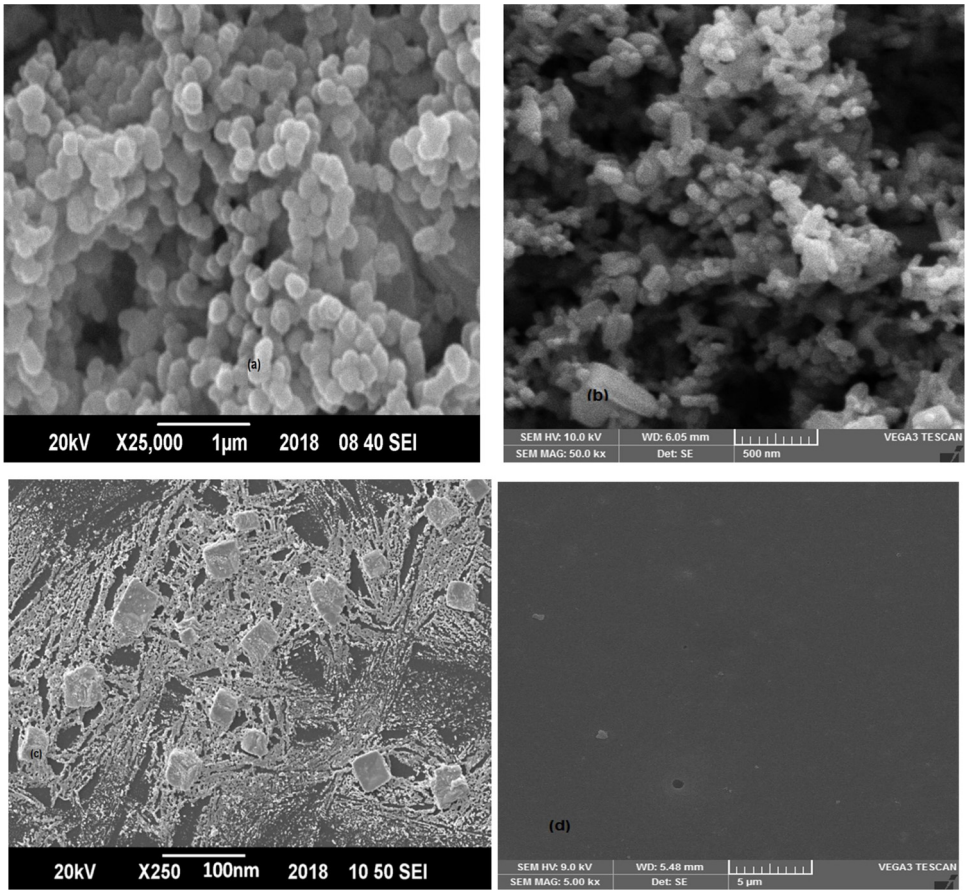

Fig. 3. (a) SEM image of compact TiO_2. (b) SEM image of mesoporous TiO_2. (c) SEM image of $CH_3NH_3PbBr_3$. (d) SEM image of Spiro-OMeTAD.

titanium dioxide nanoparticles in compact layer is calculated to be 69 nm as shown in Fig. 4a.

The surface morphology of Mesoporous titanium dioxide layer deposited on compact TiO_2 is shown below in Fig. 3b. Some dark areas in morphology are pinholes present in the layer. These holes do not affect the efficiency of the solar cell as the mesoporous layer is deposited on compact TiO_2 layer. Average particle size of the mesoporous titanium dioxide nanoparticles is calculated to be 65 nm as shown in Fig. 4b.

SEM image in Fig. 3(c) shows the monocrystalline structures of Perovskite, $CH_3NH_3PbBr_3$. Prominent cuboid structures randomly dispersed in thin film are shown in image. Size of cuboids formed depends upon heating time during fabrication step. After spin coating, the deposited film was heated at 150 °C for 50 min. Size would be bigger if heating time was increased from 50 min to several hours. Histogram in Fig. 4(c) shows calculated average particle size (69 nm) of $CH_3NH_3PbBr_3$. SEM image of Spiro-OMeTAD in Fig. 3(d) shows a uniform layer with no visible crystal structure. Spiro-OMeTAD always shows a very smooth homogenous surface without any specific shape within micrometer to nanometer range. Film of spiro-OMeTAD always consists of few holes which are due to additives used for dilution. Usually large numbers of holes are observed in the film when other additives such as chlorobenzene, dichlormethane, toluene etc are used [17]. But only few holes are seen in the SEM image due to addition of dimethyl formamide (DMF).

The materials functionality in solar cell mainly depends upon absorption properties. UV–vis spectroscopy analysis was performed to analyze the optical properties such as amount of light absorption and band gap value of all layers. This analysis helps determining the light absorbance in ultraviolet and visible region. The electrons get excited after absorption of light takes place. Fig. 5(a)–(d) shows UV–vis absorption spectra for compact TiO_2, mesoporous TiO_2, $CH_3NH_3PbBR_3$ and Spiro-OMeTAD respectively. Different values of absorption are determined along a spectrum of wavelength. The UV analysis determines the amount of absorbed radiations in UV and visible range.

Tauc plot of $(\alpha h\nu)^2$ versus $h\nu$ was drawn to determine band gap value. Band gap values calculated for compact TiO_2, mesoporous TiO_2, $CH_3NH_3PbBr_3$ and spiro-OMeTAD are 3.2 eV, 3.4 eV, 2.09 eV and 2.74 eV respectively as shown in Fig. 6(a)–(d). These band gap values meet the criteria of band gap alignment for solar cell structure.

To find power conversion efficiency (PCE) IV curve for all four devices was found using solar simulator. Fig. 7(a)–(d) shows IV curve for all four devices.

From IV curve efficiency parameters i.e. short circuit current (Isc), open voltage current (Voc), current at maximum power (Imp)

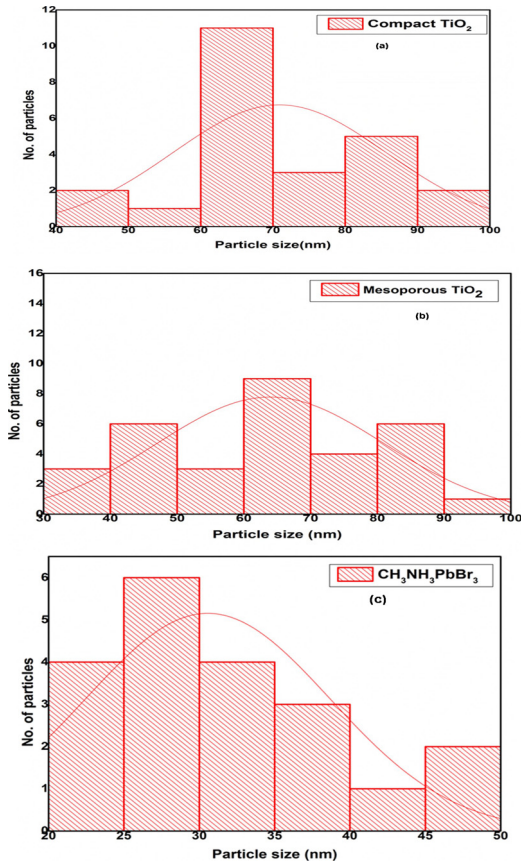

Fig. 4. Histogram for particle size. (a) Compact TiO_2. (b) Mesoporous TiO_2. (c) $CH_3NH_3PbBr_3$.

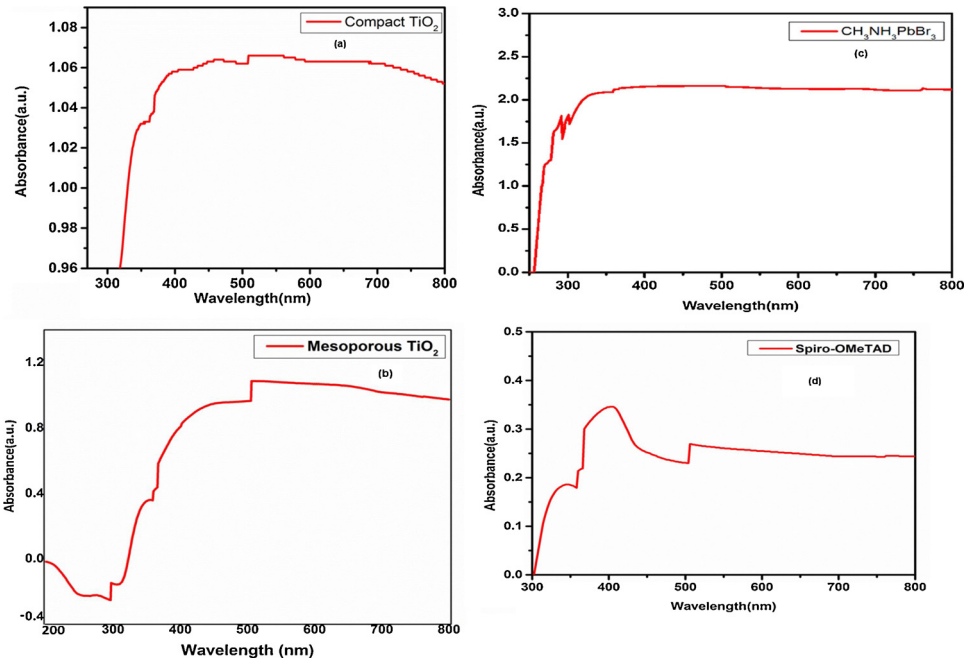

Fig. 5. (a) UV–vis absorption spectra of compact TiO2. (b) UV–vis absorption spectra of mesoporous TiO2. (c) UV–vis absorption spectra of CH3NH3PbBr3. (d) UV–vis absorption spectra of Spiro-OMeTAD.

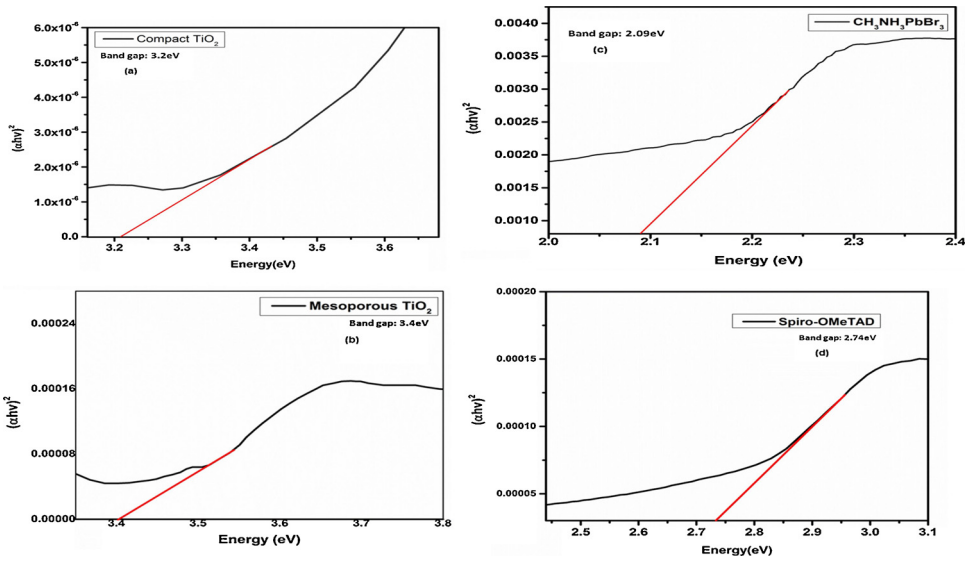

Fig. 6. Tauc plot for band gap. (a) Compact TiO_2. (b) Meoporous TiO_2. (c) $CH_3NH_3PbBr_3$. (d) spiro-OMeTAD.

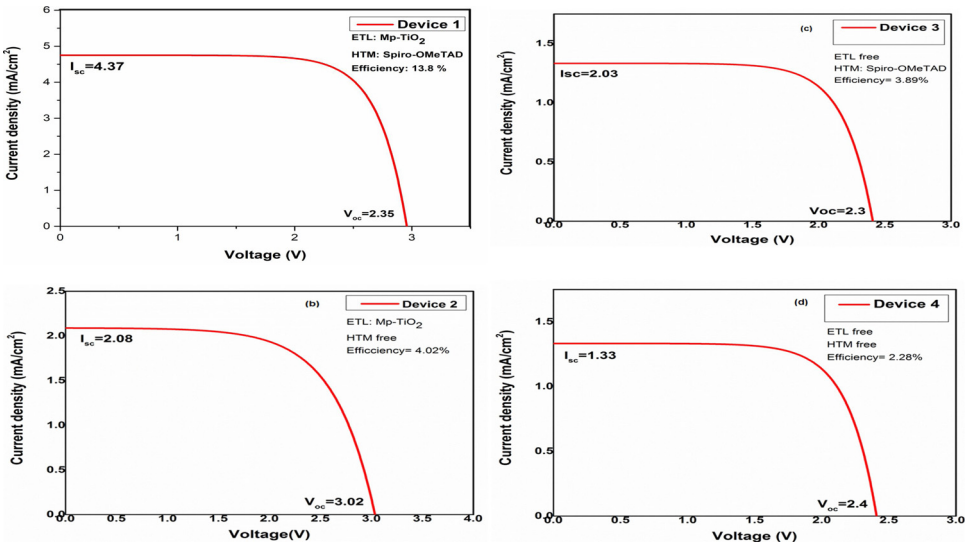

Fig. 7. IV curves of (a) Device 1. (b) D evice 2. (c) Device 3. (d) Device 4.

and voltage at maximum power (Vmp) were calculated. Efficiency comparison of all devices tells us that the maximum efficiency is obtained by using spiro-OMeTAD as HTM and mesoporous TiO2 as ETL (device1,η = 13.8 %). Mesoporous structure is sponge like having pores of size 2 − 50 nm. Due to presence of nano pores in mesoporous structure of TiO_2 the perovskite material gets penetrated into ETL providing maximum sites for efficient electron transfer [18]. Second highest PCE (η = 4.02 %) is obtained with device 2 which is HTM free and mesoporous TiO_2 as ETL is used. Holes transportation is possible even without the deposition of HTM layer because perovskite material itself acts as HTM. But holes transfer with perovskite is not as efficient as it is with spiro-OMeTAD (HTM). Therefore efficiency is decreased in the absence of spiro-OMeTAD. However, stability problems are resolved without spiro OMeTAD. PCEs obtained of ETL free devices with and without HTM layer were less than devices which have ETL layers. PCE of device 3 (only compact TiO_2 in place of mesoporous TiO_2 (ETL) and spiro-OMeTAD as HTM) is higher than device 4 (both ETL and HTM free). PCE difference here is again due to the presence of HTM which makes holes transportation easier. Absence of ETL and HTM layer in device 4 makes it least efficient as compared to first three devices. Although PCE obtained by device 4 is least but still HTM and ETL free architectures are promising and necessitates optimizations to become future low cost and highly efficient PSCs. All efficiency parameters along with calculated PCEs are given in Table 1.

Table 1
Efficiency parameters calculated from IV curve.

Name	ETL	HTM	J_{sc} (mA cm^{-2})	V_{oc} (V)	FF	PCE (%)
Device 1	Mesoporous TiO2	Spiro-OMeTAD	4.37	1.35	0.52	13.8
Device 2	Mesoporous TiO2	HTM free	2.08	1.5	0.64	4.02
Device 3	ETL free (Comp-TiO2)	Spiro-OMeTAD	2.03	1.3	0.83	3.89
Device 4	ETL free (Comp-TiO2)	HTM free	1.33	1.4	0.71	2.28

3. Conclusion

All four devices were fabricated successfully by addition and elimination of electron transport layer (ETL) and hole transport layer (HTM). XRD analysis confirmed the synthesis of required crystalline structured compact TiO_2, mesoporous TiO_2 and perovskite material. Scanning electron microscope (SEM) images have shown the desired surface morphology for all layers. Bandgap values calculated from UV graphs fulfilled the desired criteria for device structure. IV graph was plotted for each device to make efficiency comparison. Presence of both ETL and HTM layers resulted into maximum PCE efficiency of 13.8 %. Maximum efficiency was obtained because charge carriers were transferred more efficiently in the presence of both ETL and HTM layers. By elimination of HTM in second device PCE decreased to 4.02 %. Although holes were transferred by perovskite layer but transfer mechanism was not as efficient as it was in the presence of HTM layer. Mesoporous structure of TiO_2 proved to be very beneficial for inceease in PCE. Its mesoporous structure provided maximum cotes for the electron interaction and transfer. Perovskite material got absorbed into the mesoscopic layer through the pores present in its structure. In the third device HTM layer was present but ETL was removed. This structural combination resulted into 3.89 % PCE. Compact TiO2 which is actually a blocking layer also acted as ETL. In the fourth device both ETL and HTM layers were removed. PCE calculated was 2.28 %. PCE of device 4 has reduced but is not zero which confirms the successful working of cell. Reduction in efficiencies due to elimination of ETL and HTM could be enhanced by more research work in future. While HTM and ETL free PSCs which enables low cost and simple fabrication are emerging but further study on enhancing photovoltaic parameters is necessary. Due to stability issues PSCs requires more research to find ways to make devices stabilized to get commercialized.

Declaration of Competing Interest

The authors declare that there are no conflicts of interest.

Acknowledgements

This work was supported by ORIC and Physics department, Forman Christian College (A Chartered University), Lahore, Pakistan.

References

[1] L. Huang, X. Sun, C. Li, et al., Electron transport layer-free planar perovskite solar cells: further performance enhancement perspective from device simulation, Sol. Energy Mater. Sol. Cells 157 (2016) 1038–1047.
[2] Qiqi He, Kai Yao, Xiaofeng Wang, et al., Room-temperature and solution-processable Cu-doped nickel oxide nanoparticles for efficient hole-transport layers of flexible large-area perovskite solar cells, ACS Appl. Mater. Interfaces 48 (2017) 41887–41897.
[3] Francesco Di Giacomo, Azhar Fakharuddin, et al., Progress, challenges and perspectives in flexible perovskite solar cells, Energy Environ. Sci. 10 (2016) 3007–3035.
[4] L. Etgar, Hole-transport material-free perovskite-based solar cells, MRS Bull. 8 (2015) 674–680.
[5] L. Lin, L. Jiang, et al., Simulation of optimum band structure of HTM-free perovskite solar cells based on ZnO electron transporting layer, Mater. Sci. Semicond. Process. 90 (2019) 1–6.
[6] Dianyi Liu, Jinli Yang, Timothy L. Kelly, Compact layer free perovskite solar cells with 13.5% efficiency, J. Am. Chem. Soc. 49 (2014) 17116–17122.
[7] R. Songtanasit, T. Taychatanapat, S. Chatraphorn, Electrical properties of ultra-thin TiO2 compact layer on FTO for perovskite solar cells, J. Phys. Conf. Ser. 901 (12161) (2017).
[8] Chenxi Zhang, Yudan Luo, et al., Influence of different TiO2 blocking films on the photovoltaic performance of perovskite solar cells, Appl. Surf. Sci. 388 (2016) 82–88.
[9] C.V.V.M. Gopi, M. Venkata-Haritha, et al., Low-temperature easy-processed carbon nanotube contact for high-performance metal-and hole-transporting layer-free perovskite solar cells, J. Photochem. Photobiol. A: Chem. 332 (2017) 265–272.
[10] Chenxi Zhang, Yudan Luo, et al., Influence of different TiO2 blocking films on the photovoltaic performance of perovskite solar cells, Appl. Surf. Sci. 388 (2016) 82–88.
[11] Eran Edri, Saar Ki rmayer, Michael Kulbak, et al., Chloride inclusion and hole transport material doping to improve methyl ammonium lead bromide perovskite-based high open-circuit voltage solar cells, J. Phys. Chem. Lett. 4 (2014) 429–433.
[12] Akihiro Kojima, Kenjiro Teshima, Yasuo Shirai, et al., Organometal halide perovskites as visible-light sensitizers for photovoltaic cells, J. Am. Chem. Soc. 131 (2009) 6050–6051.
[13] J. Stenberg, Perovskite Solar Cells, (2017).
[14] S.S. Mali, C.S. Shim, et al., Highly stable and efficient solid-state solar cells based on methylammonium lead bromide (CH 3 NH 3 PbBr 3) perovskite quantum dots, NPG Asia Mater. 7 (2015) 208.
[15] Yafang Wang, Liping Li, et al., New insights into fluorinated TiO 2 (brookite, anatase and rutile) nanoparticles as efficient photocatalytic redox catalysts, RSC Adv. 43 (2015) 34302–34313.
[16] Hui Tong, Naoya Enomoto, Miki Inada, et al., Synthesis of mesoporous TiO2 spheres and aggregates by sol–gel method for dye-sensitized solar cells, Mater. Lett. 141 (2015) 259–262.
[17] L.K. Ono, Z. Hawash, E.J. Juarez-Perez, et al., The influence of secondary solvents on the morphology of a spiro-MeOTAD hole transport layer for lead halide perovskite solar cells, J. Phys. D Appl. Phys. 51 (2018) 294001.
[18] H.J. Snaith, Perovskites: the emergence of a new era for low-cost, high-efficiency solar cells, J. Phys. Chem. Lett. 21 (2013) 3623–3630.